Supporting Information

Achieving an Optimal Performance Balance in UV Nonlinear Optical Crystals via Hydrogen-Bond Regulation

Shuai An[a, b], Yaqi Jin[a], Wenhu Wang[a], Bailin Chen[a, b], Zhihua Yang[a, b],

Xueling Hou[a, b]* and Shilie Pan[a, b]*

[a]Research Center for Crystal Materials; CAS Key Laboratory of Functional Materials and Devices for Special Environmental Conditions; Xinjiang Key Laboratory of Functional Crystal Materials; Xinjiang Technical Institute of Physics and Chemistry, Chinese Academy of Sciences, 40-1 South Beijing Road, Urumqi 830011, China.

[b]Center of Materials Science and Optoelectronics Engineering, University of Chinese Academy of Sciences, Beijing 100049, China.

*Corresponding authors, E-mails: xlhou@ms.xjb.ac.cn; slpan@ms.xjb.ac.cn.

Experimental procedures

Reagents. $C_2NO_2H_5$ (>98 %, Macklin), CF_3SO_3H (98 %, Macklin). All commercial reagents are used directly without purification.

[$C_2NO_2H_6$][SO_3CF_3] (I) crystal synthesis method:

Growth of crystals using the aqueous solution evaporation method: $C_2NO_2H_5$ and CF_3SO_3H were uniformly mixed at a 1:1 molar ratio and placed in a 100 mL PTFE beaker. then add deionized water and stir to form the solution. Solvent evaporation was then conducted at room temperature until crystal growth was complete, yielding millimeter-scale crystals.

[$C_4N_2O_4H_{11}$][SO_3CF_3] (II) crystal synthesis method:

Growth of nonlinear optical crystals using the aqueous solution evaporation method: a. Uniformly mix components $C_2NO_2H_5$ and CF_3SO_3H in an 8:3 molar ratio, transfer the mixture into a 500 mL PTFE beaker, then add deionized water and stir to form the solution; b. Heat the water bath to 60-70 °C, then place the beaker in the bath for 14 days of constant-temperature solvent evaporation. After crystal growth is complete, a crystal with the sizes up to 18mm × 4mm × 2mm was obtained.

Single-crystal X-ray diffraction.

For the structural characterization of the as-synthesized samples, plate-shaped single crystals of the target compounds with appropriate dimensions were selected under an optical microscope. Single-crystal X-ray diffraction data for the two compounds were obtained using a Bruker D8 Venture diffractometer. This diffractometer was equipped with monochromatic Mo-Kα (λ = 0.71073 Å) and Cu-Kα (λ = 1.54056 Å) radiations as the sources. Data integration was carried out via the Bruker SAINT program. [1] The crystal structures of the two compounds were solved by the direct method and refined using the SHELXTL system within the Olex2 software environment. [2] All atomic positions were refined employing full-matrix least-squares methods. The PLATON program was utilized to validate these structures, and no suggestion of higher symmetry was obtained.

Powder X-ray diffraction.

Powder samples were placed on a suitable tray, after which powder X-ray diffraction data were collected using a Bruker D2 PHASER diffractometer. The diffractometer employed Cu Kα radiation (λ = 1.5418 Å) and operated at 300 K. Diffraction patterns were recorded over a 2θ range of 5-70 °. To verify the purity of the samples, the experimental diffraction pattern was compared with a theoretically simulated powder pattern.

This simulated pattern was generated by calculating the crystal plane positions and crystalline interplanar spacings from the previously obtained crystal data. Through this comparison, it is confirmed that the polycrystalline powder samples of the two compounds exhibit sufficient purity for subsequent tests.

Optical spectroscopies.

The sample was pretreated by mixing it with dried, highly purified KBr at a mass ratio of 4 mg (sample) to 300 mg (KBr). After pretreatment, its IR spectrum was collected at room temperature using a Shimadzu IR Affinity-1 Fourier transform infrared spectrometer, with data recorded over a wavelength range of 400-4000 cm^{-1}. Separately, the single-crystal transmission spectrum was measured at room temperature via a Shimadzu SolidSpec-3700DUV spectrophotometer, covering a wavelength range of 190-1600 nm.

Thermal analysis.

The sample's thermogravimetric and differential scanning calorimetry (TG-DSC) analysis was performed on a simultaneous thermal analyzer. Polycrystalline samples were loaded into a Pt crucible, followed by heating to 600 °C at 5 °C/min in a flowing nitrogen environment.

Refractive index measurements.

The immersion technique was used to determine the birefringence of the sample, with a GR-5 Gem Refractometer employed for the measurement. The refractometer operated at a wavelength of 589.3 nm (yellow light). During the experiment, the maximum and minimum refractive indices were measured using an unpolished wafer.

Powder second harmonic generation measurement.

Powder second-harmonic generation (SHG) tests were conducted using a modified Kurtz-Perry method. The excitation source was a Q-switched Nd:YVO_4 solid-state laser operating at 1064 nm. Polycrystalline samples were first ground and then sieved to obtain fractions with distinct particle size ranges: 25-45, 45-58, 58-75, 75-106, 106-150, and 150-212 μm. For reference purposes, microcrystalline potassium dihydrogen phosphate (KDP) samples were also sieved into the same particle size ranges, and each range of KDP was used as the corresponding reference for SHG measurements.

Hirshfeld surface analysis

Molecular Hirshfeld surfaces and related 2D fingerprint plots of $(C_2NO_2H_5)$ CF_3SO_3 and $(C_4N_2O_4H_{11})$ CF_3SO_3 were produced using a CIF file to analyze the crystal structures generated by the Crystal Explorer program.[3] The normalized contact distance (d_{norm}) depends on the atom's d_i and de (the distance from Hirshfeld surface to the nearest nucleus inside and outside, respectively) as well as the van der Waals radii of the atoms given by the equation (1).

$$d_{norm} = \frac{d_i - r_i^{vdw}}{r_i^{vdw}} + \frac{d_e - r_e^{vdw}}{r_e^{vdw}} \qquad (1)$$

Where r_i^{vdW} and r_e^{vdw} are the van der Waals radii of the atoms internal and external to the surface, respectively

Computational descriptions.

The first principles calculations for the compounds in this work were carried out by using the plane wave density functional theory (DFT) package CASTEP. [4-5] In addition, the gradient approximation (GGA)-based Perdew-Burke-Ernzerhof (PBE) functional was used, with core-valence interactions computed via the norm-conserving pseudopotential (NCP).[6-7] Since GGA often underestimates the band gap—arising from the discontinuity of exchange-correlation energy—the Heyd-Scuseria-Ernzerhof (HSE06) hybrid functional[8] was employed to yield more precise band gap results. Thus, the band gap difference between the GGA and HSE06 methods served as a scissor operator for optical property calculations. The plane wave cutoff energy was set to 900 eV, and self-consistent field (SCF) calculations were performed with a total energy convergence criterion of 10^{-6} eV/atom. Each material had a k-point separation of 0.04 $Å^{-1}$ in the Brillouin zone, producing the respective Monkhorst-Pack k-point meshes. All other calculation parameters and convergence criteria used the default settings of the CASTEP package. We calculated the molecular orbitals and polarizability anisotropy of the $[C_2NO_2H_6]^+$ and $[C_2NO_2H_5]$ units using density functional theory (DFT). The calculations were conducted in Gaussian 09 at the B3LYP/6-31G level of theory. [9-11] The scissor-corrected electronic band structure was used to obtain the linear optical parameters (refractive indices and birefringence) from the real part of the dielectric function. Subsequently, the SHG coefficients were calculated by applying the Aversa and Sipe length-gauge formalism at the zero-frequency limit, where the static second-order nonlinear susceptibilities originate from virtual electron (VE) and virtual hole (VH) processes. Finally, the specific contribution of ionic groups to the NLO coefficients (d_{ij}) was isolated using the real-space atom-cutting method.

$$\chi_{\alpha\beta\gamma}^{(2)} = \chi_{\alpha\beta\gamma}^{(2)}(\mathrm{VE}) + \chi_{\alpha\beta\gamma}^{(2)}(\mathrm{VH})$$

where $\chi_{\alpha\beta\gamma}^{(2)}(\mathrm{VE})$ and $\chi_{\alpha\beta\gamma}^{(2)}(\mathrm{VH})$ are computed with the following formulas:

$$\chi_{\alpha\beta\gamma}^{(2)}(\mathrm{VE}) = \frac{e^3}{2\hbar^2 m^3}\sum_{\mathrm{vcc'}}\int\frac{d^3k}{4\pi^3}P(\alpha\beta\gamma)\mathrm{Im}[P_{cv}^{\alpha}P_{cc'}^{\beta}P_{c'v}^{\gamma}]\left(\frac{1}{\omega_{cv}^3\omega_{vc'}^2}+\frac{2}{\omega_{vc}^4\omega_{c'v}^2}\right)$$

$$\chi_{\alpha\beta\gamma}^{(2)}(\mathrm{VH}) = \frac{e^3}{2\hbar^2 m^3}\sum_{\mathrm{vv'c}}\int\frac{d^3k}{4\pi^3}P(\alpha\beta\gamma)\mathrm{Im}[P_{vv'}^{\alpha}P_{cv'}^{\beta}P_{cv}^{\gamma}]\left(\frac{1}{\omega_{cv}^3\omega_{v'c}^2}+\frac{2}{\omega_{vc}^4\omega_{cv'}^2}\right)$$

Table S1 Crystal data and structure refinement for **$[C_2NO_2H_6][SO_3CF_3]$ (I) and $[C_4N_2O_4H_{11}][SO_3CF_3]$ (II).**

	$[C_2NO_2H_6][SO_3CF_3]$	$[C_4N_2O_4H_{11}][SO_3CF_3]$
Formula weight	225.15	300.22
Temperature [K]	296.15	296.15
Crystal system	triclinic	monoclinic
Space group (number)	$P\bar{1}$ (2)	Cc (9)
a [Å]	5.2953(8)	14.8353(5)
b [Å]	7.1724(9)	8.9818(3)
c [Å]	11.1488(15)	10.0267(4)
α [°]	107.573(5)	90
β [°]	91.936(5)	120.0900(10)
γ [°]	99.539(5)	90
Volume [Å^3]	396.50(10)	1155.99(7)
Z	2	4
ρ_{calc} [gcm^{-3}]	1.886	1.725
μ [mm^{-1}]	0.457	0.352
F (000)	228	616
Radiation	MoK_α (λ=0.71073 Å)	MoK_α (λ=0.71073 Å)
2θ range [°]	6.06 to 55.25 (0.77 Å)	5.54 to 54.94 (0.77 Å)
Index ranges	$-6 \leq h \leq 6$ $-9 \leq k \leq 9$ $-14 \leq l \leq 14$	$-19 \leq h \leq 18$ $-11 \leq k \leq 11$ $-13 \leq l \leq 13$
Reflections collected	17367	4328
Independent reflections	1833 R_{int} = 0.0447 R_{sigma} = 0.0245	2362 R_{int} = 0.0640 R_{sigma} = 0.0810
Data / Restraints / Parameters	1833/0/122	2362/2/166
Absorption correction T_{min}/T_{max} (method)	0.7245/0.7456 (none)	0.6298/0.7456 (none)
Goodness-of-fit on F^2	0.919	0.973
Final R indexes [$I \geq 2\sigma(I)$]	R_1 = 0.0394 wR_2 = 0.1352	R_1 = 0.0476 wR_2 = 0.0917
Final R indexes [all data]	R_1 = 0.0445 wR_2 = 0.1462	R_1 = 0.0756 wR_2 = 0.1039
Largest peak/hole [eÅ^{-3}]	0.53/-0.56	0.21/-0.27

Table S2 Fractional atomic coordinates (×10[4]) and equivalent isotropic displacement parameters (Å[2]×10[3]) for **I** and **II** .

$[C_2NO_2H_6][SO_3CF_3]$				
Atom	***X***	***Y***	***z***	U_{eq}
S1	0.08658(8)	0.30446(7)	0.14857(4)	0.0329(2)
N1	0.5065(4)	0.8277(3)	0.10739(16)	0.0390(4)
O1	0.4080(3)	0.9635(3)	0.34854(14)	0.0470(4)
O2	0.7636(3)	0.8897(3)	0.42183(14)	0.0493(4)
O3	0.2164(5)	0.4558(3)	0.10093(19)	0.0684(6)
O4	0.1873(3)	0.2672(3)	0.13046(18)	0.0598(5)
O5	0.1995(3)	0.1289(3)	0.11458(15)	0.0478(4)
F1	0.0711(5)	0.5729(3)	0.36271(18)	0.0864(7)
F2	0.0514(4)	0.2795(3)	0.37444(15)	0.0729(6)
F3	0.4069(4)	0.4440(3)	0.34975(18)	0.0853(7)
C1	0.6959(4)	0.8195(3)	0.20439(18)	0.0351(4)
C2	0.6058(4)	0.9000(3)	0.33365(17)	0.0327(4)
C3	0.1576(5)	0.4064(3)	0.3189(2)	0.0443(5)

$[C_4N_2O_4H_{11}][SO_3CF_3]$

Atom	*X*	*Y*	*z*	U_{eq}
S1	0.34366(10)	0.78464(15)	0.33424(14)	0.0382(3)
N1	0.4741(3)	0.5864(6)	0.7613(5)	0.0410(12)
O1	0.7558(3)	0.0547(4)	0.6539(4)	0.0539(9)
O2	0.6202(3)	0.1832(4)	0.4776(4)	0.0371(9)
O3	0.6338(3)	0.3277(4)	0.6971(4)	0.0402(10)
O4	0.4724(3)	0.4078(4)	0.5432(4)	0.0374(9)
O5	0.3419(3)	0.7080(5)	0.4579(4)	0.0508(11)
F1	0.3308(3)	1.0286(5)	0.4632(5)	0.0741(13)
F2	0.4854(3)	0.9590(5)	0.5346(5)	0.0793(14)
F3	0.3922(4)	1.0599(5)	0.3123(5)	0.0830(14)
C1	0.6701(4)	0.0270(6)	0.3952(6)	0.0348(12)
C2	0.6873(4)	0.0755(6)	0.5236(5)	0.0274(10)
C3	0.5543(4)	0.4075(5)	0.6665(5)	0.0280(11)
C4	0.5718(4)	0.3094(6)	0.7960(6)	0.0340(12)
C5	0.3900(5)	0.9689(7)	0.4134(7)	0.0485(15)

Table S3 Selected bond lengths and bond angles for **I** and **II** .

$[C_2NO_2H_6][SO_3CF_3]$			
Atom-Atom	**Length [Å]**	**Atom-Atom**	**Length [Å]**
S1-O5	1.436(16)	O1-C2	1.207(2)
S1-O4	1.426(17)	F2-C3	1.312(3)
S1-O3	1.434(19)	N1-C1	1.471(3)
S1-C3	1.818(2)	F3-C3	1.315(3)
O2-C2	1.296(2)	F1-C3	1.311(3)
$[C_4N_2O_4H_{11}][SO_3CF_3]$			
Atom-Atom	**Length [Å]**	**Atom-Atom**	**Length [Å]**
S1-O5	1.430(4)	F1-C5	1.322(7)
S1-O7	1.433(4)	F2-C5	1.328(7)
S1-O6	1.437(4)	F3-C5	1.316(7)
S1-C5	1.815(6)	N2-C1	1.482(6)
O2-C2	1.296(6)	N1-C4	1.481(6)
O4-C3	1.224(6)	C3-C4	1.502(7)
O3-C3	1.279(6)	C1-C2	1.496(7)

$[C_2NO_2H_6][SO_3CF_3]$			
Atom-Atom-Atom	**Angle [°]**	**Atom-Atom-Atom**	**Angle [°]**
O5-S1-C3	104.12(10)	O2-C2-C1	111.79(16)
O4-S1-O5	114.58(12)	O1-C2-O2	126.18(17)
O4-S1-O3	115.67(14)	F1-C3-S1	110.63(17)
O4-S1-C3	104.25(11)	F1-C3-F2	108.8(2)
O3-S1-O5	112.14(13)	F1-C3-F3	108.1(2)
$[C_4N_2O_4H_{11}][SO_3CF_3]$			
Atom-Atom-Atom	**Angle [°]**	**Atom-Atom-Atom**	**Angle [°]**
O5-S1-O7	114.6(3)	N1-C4-C3	110.9(4)
O5-S1-O6	115.3(3)	F1-C5-S1	110.9(4)
O5-S1-C5	103.1(3)	F1-C5-F2	106.7(5)
O7-S1-O6	113.4(3)	F2-C5-S1	109.6(4)
O7-S1-C5	104.7(3)	F3-C5-S1	112.4(4)
O6-S1-C5	103.7(3)	F3-C5-F1	108.5(6)
O4-C3-O3	125.0(5)	F3-C5-F2	108.7(5)

Table S4 Hydrogen atom coordinates (Å×10^4) and isotropic displacement parameter (Å^2×10^3) for **I** and **II**.

$[C_2NO_2H_6][SO_3CF_3]$				
Atom	***X***	***y***	***z***	U_{eq}
H1A	0.552833	0.058962	0.865979	0.048
H1B	0.419456	0.178553	0.963819	0.048
H1C	0.623798	0.274657	0.906886	0.048
H1D	0.282641	0.316999	0.809868	0.043
H1E	0.139369	0.102355	0.800776	0.043

$[C_4N_2O_4H_{11}][SO_3CF_3]$				
Atom	***X***	***y***	***z***	U_{eq}
H1A	0.604150	0.078199	0.357635	0.041
H1B	0.666209	0.030970	0.310874	0.041
H1C	0.445308	0.626708	0.667701	0.049
H1D	0.488146	0.657534	0.830780	0.049
H1E	0.430061	0.521082	0.764449	0.049
H2	0.625176	0.227209	0.552630	0.056
H2A	0.735601	-0.207673	0.374029	0.045
H2B	0.766180	-0.178603	0.533824	0.045
H2C	0.811966	-0.092720	0.459825	0.045
H4A	0.597211	0.452205	0.890170	0.041
H4B	0.624352	0.582677	0.812070	0.041

Table S5 Comparison of UV and DUV NCS compounds**.**

No	Compound	Space group	Cutoff edge(nm)	Bandgap (eV)	△ncal	Shortest λ_{PM} (nm)	SHG (×KDP) exp	Ref
1	KSO_3CF_3	$P2_1$	≤159	7.79	0.017@1064nm	276	0.8	[12]
2	β-$RbSO_3CF_3$	$P2_1$	≤159	7.94	0.034@1064 nm	N\A	N\A	[12]
3	α-$RbSO_3CF_3$	*Cm*	≤159	7.81	0.035@1064 nm	N\A	N\A	[12]
4	$CsSO_3CF_3$	$P2_1$	≤159	7.85	0.027@1064 nm	N\A	N\A	[12]
5	$Ba(NH_2SO_3)_2$	$Pna2_1$	<190	7.29	0.028@546 nm	N\A	2.7	[13]
6	$Sr(NH_2SO_3)_2$	*Pc*	<190	7.32	0.027@ 546 nm	N\A	1.2	[14]
7	$Ca(NH_2SO_3)_2{\cdot}H_2O$	$P2_12_12_1$	206	5.79	0.033@ 1064 nm	N\A	0.3	[14]
8	$Cd(NH_2SO_3)_2$	$P2_12_12_1$	210	5.18	0.037@1064 nm	N\A	0.15	[15]
9	$Ba(SO_3CH_3)_2$	$Cmc2_1$	159	> 6.2	0.04@589.3 nm	177.3	1.5	[16]
10	$Cs_2Mg(NH_2SO_3)_4{\cdot}4H_2O$	*Cm*	<180	4.949	0.054@546 nm	N\A	2.3	[17]
11	$Sr(NO_3)(NH_2SO_3){\cdot}H_2O$	$Pca2_1$	290	4.10	0.0665@ 532nm	291	5.1	[18]
12	$Rb(NO_3)(SO_3NH_3)$	$Pmc2_1$	208	5.96	0.07@ 546 nm	N/A	7	[19]
13	$C(NH_2)_3SO_3F$	*R*3*m*	200	6.2	0.133@1064 nm	200	5	[20]
14	$(CN_4H_7)SO_3NH_2$	$Pca2_1$	203	6.11	0.153@546 nm	N/A	0.1	[21]
15	K(3-pySO_3)	$Pna2_1$	275	4.26	0.312@546 nm	N/A	N/A	[22]
16	$(C_2N_4H_7O)(NH_2SO_3)$	*P*1	227	4.974	0.225@1064 nm	227	6.2	[23]
17	$(C_5H_6NO)(CH_3SO_3)$	$P2_1$	252	4.64	0.216@589.3 nm	252	2.5	[24]
18	**$(C_4N_2O_4H_{11})(CF_3SO_3)$**	***Cc***	**216**	**5.25**	**0.078@532 nm**	**216**	**1**	**This Work**

Fig. S1 Calculated and experimental XRD patterns for a). **I**, b). **II** .

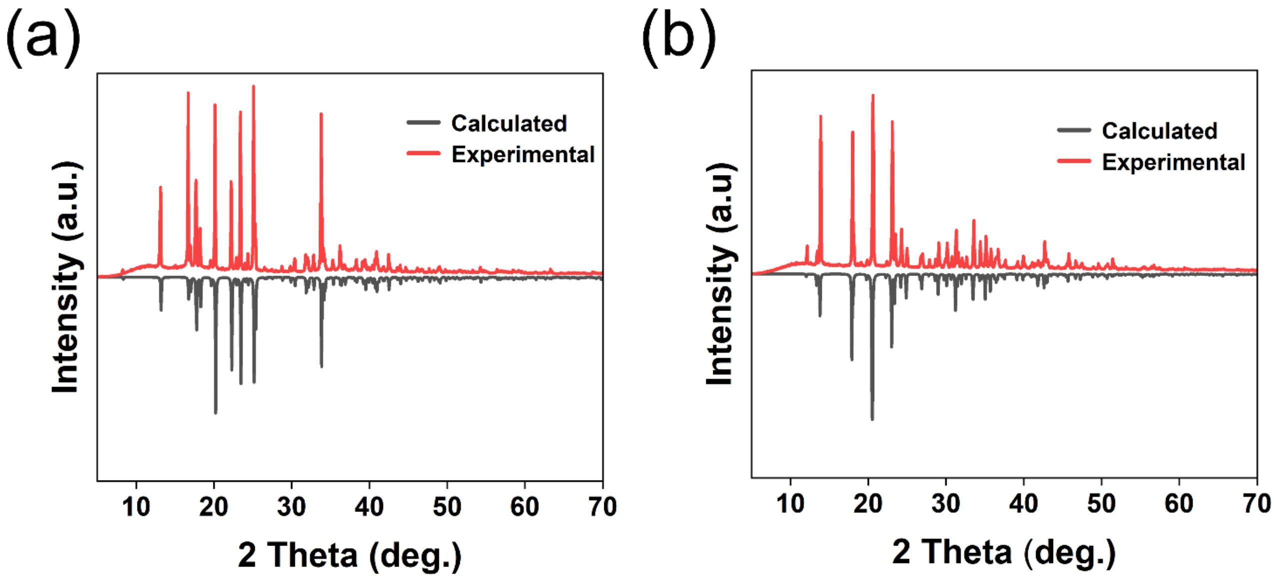

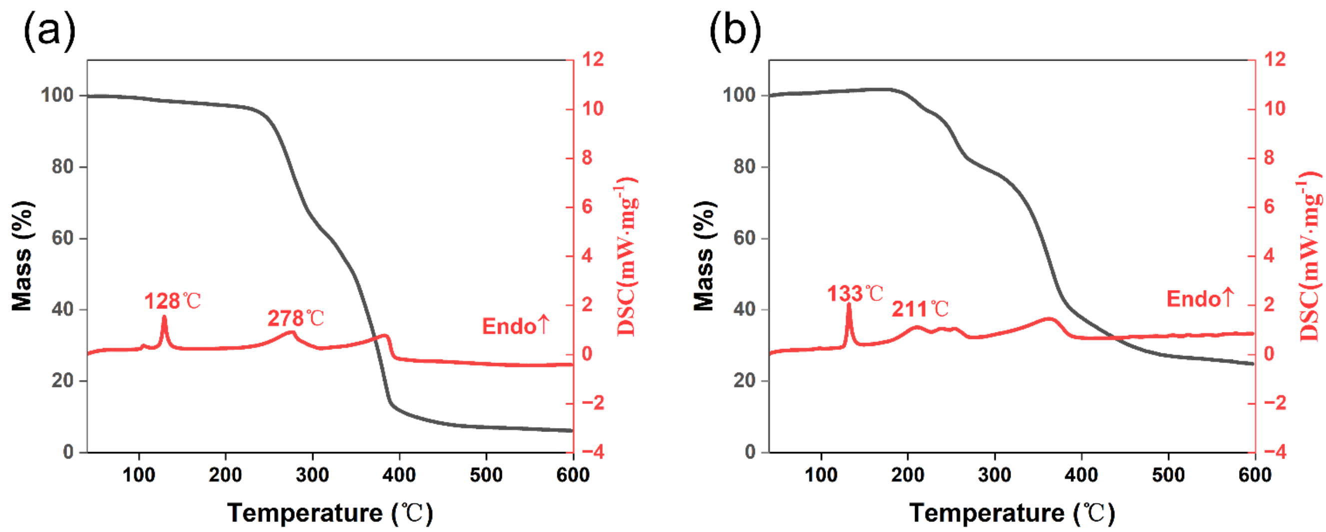

Fig. S2 TG and DSC curves of a). **I**, b). **II** under N_2 atmosphere.

Fig. S3 Transmittance spectrum of **II**.

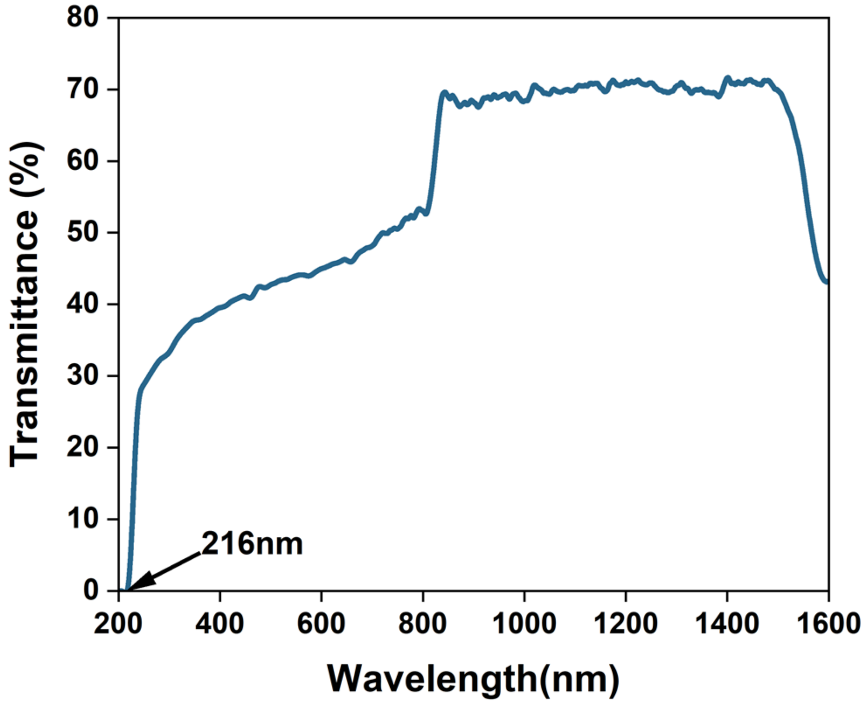

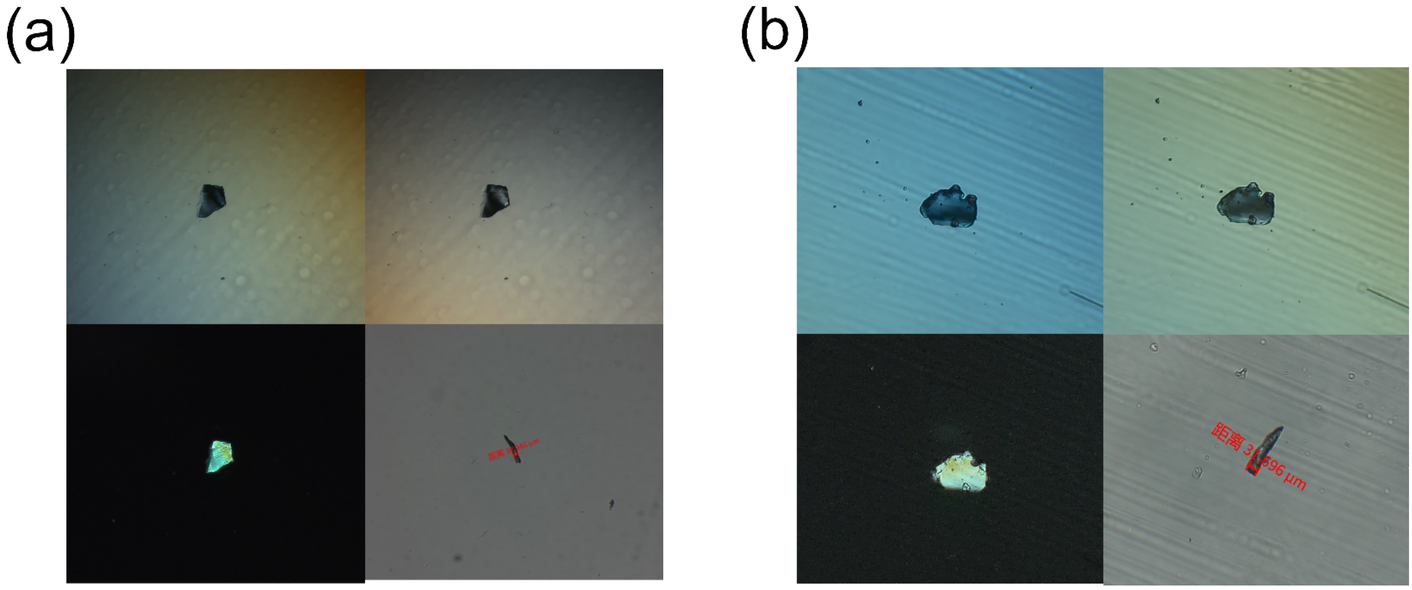

Fig. S4 Experimental refractive index difference measured at 546.1 nm for a) **I**, b). **II**.

Fig. S5 The evaluated phase-matching (PM) ability of Ⅱ based on the calculated refractive indices.

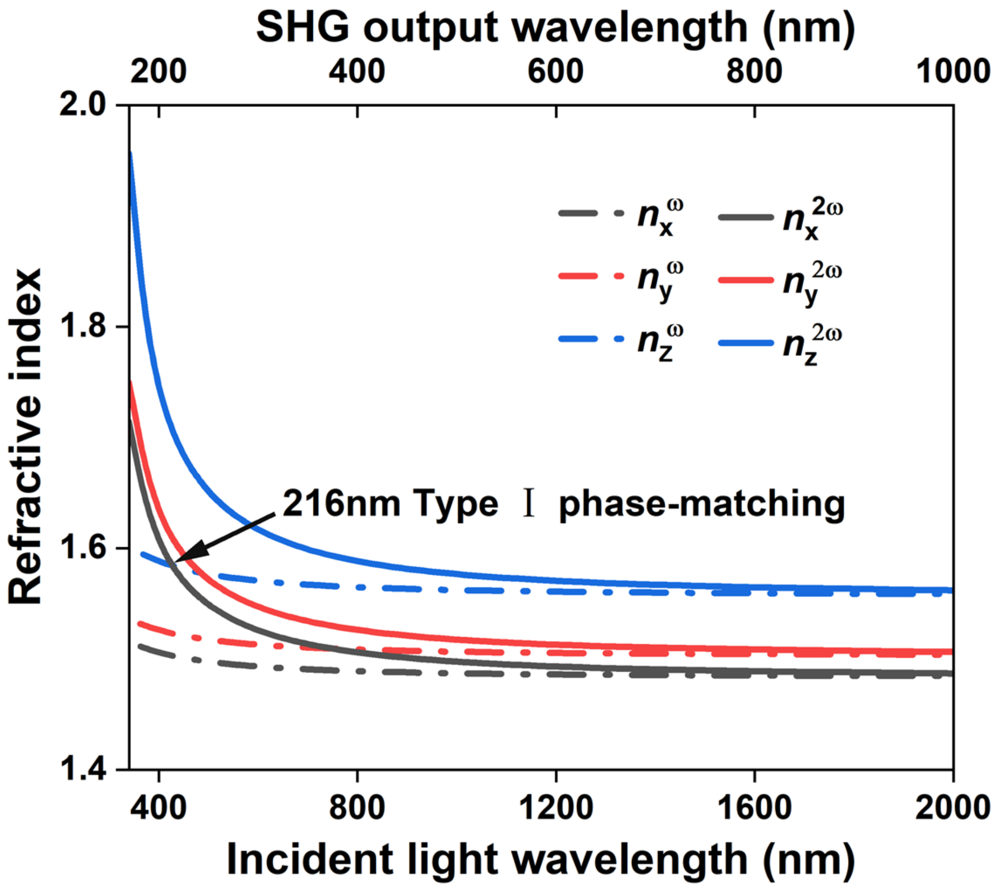

Fig S6 The IR spectra of a).**I**, b). **II**.

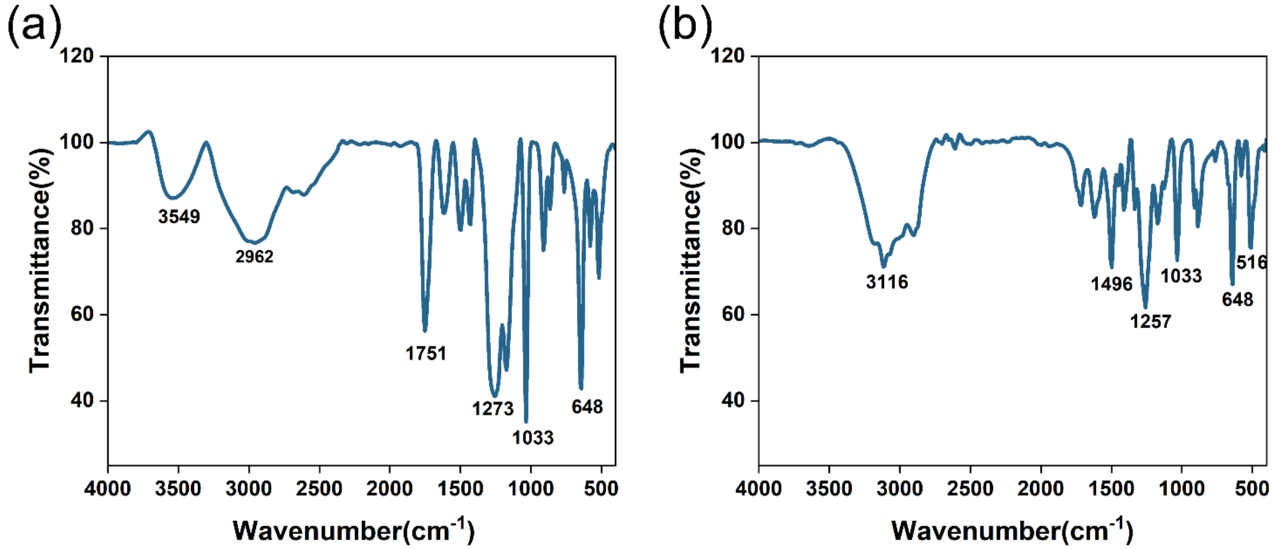

Fig. S7 Hirshfeld surfaces of a). **I**, b). **II**. (a,e) d_{norm}, (b,f) shape index, and (c,g) curvedness. (d,h) Pie-charts: relative contributions of various intermolecular interactions to the Hirshfeld surface area.

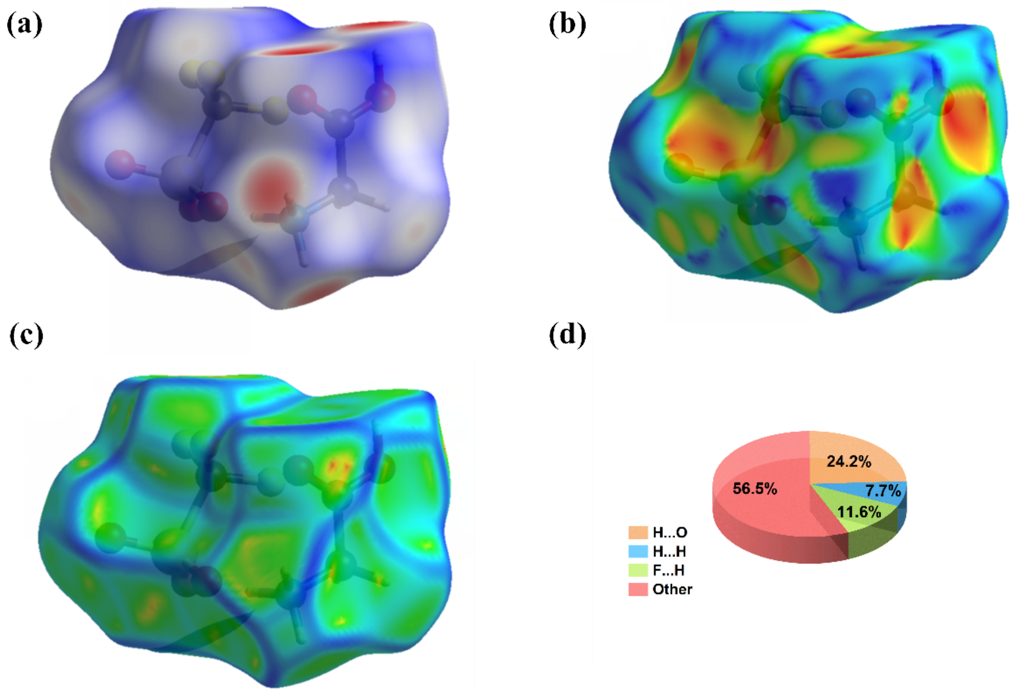

a). I

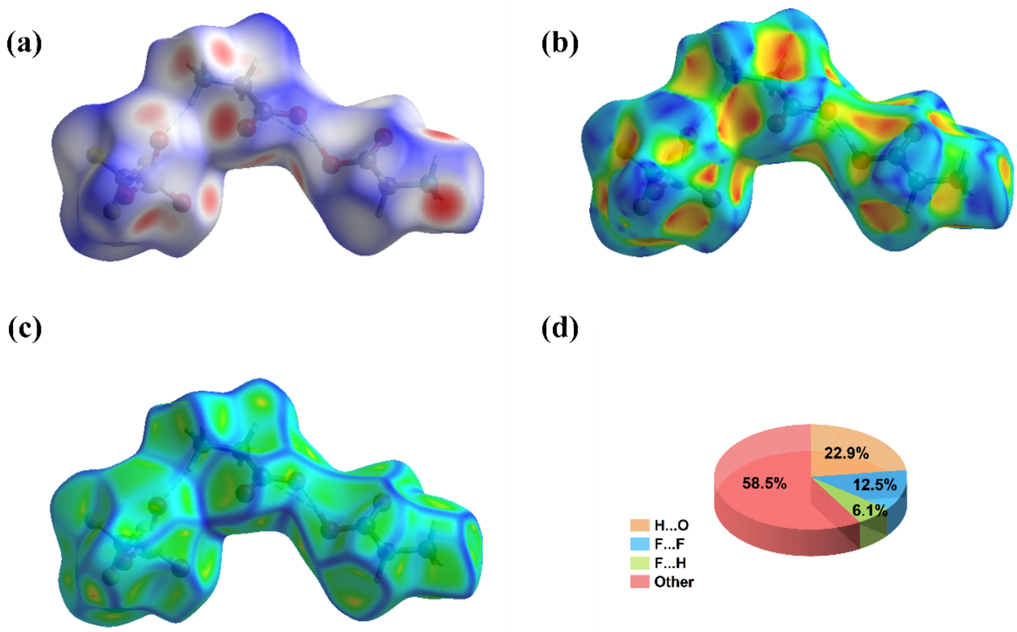

b). II

Fig. S8 2D fingerprint plots for (a) overall interactions and (b-h) individual interactions of atom types in crystal packing of A). **I**, B). **II**.

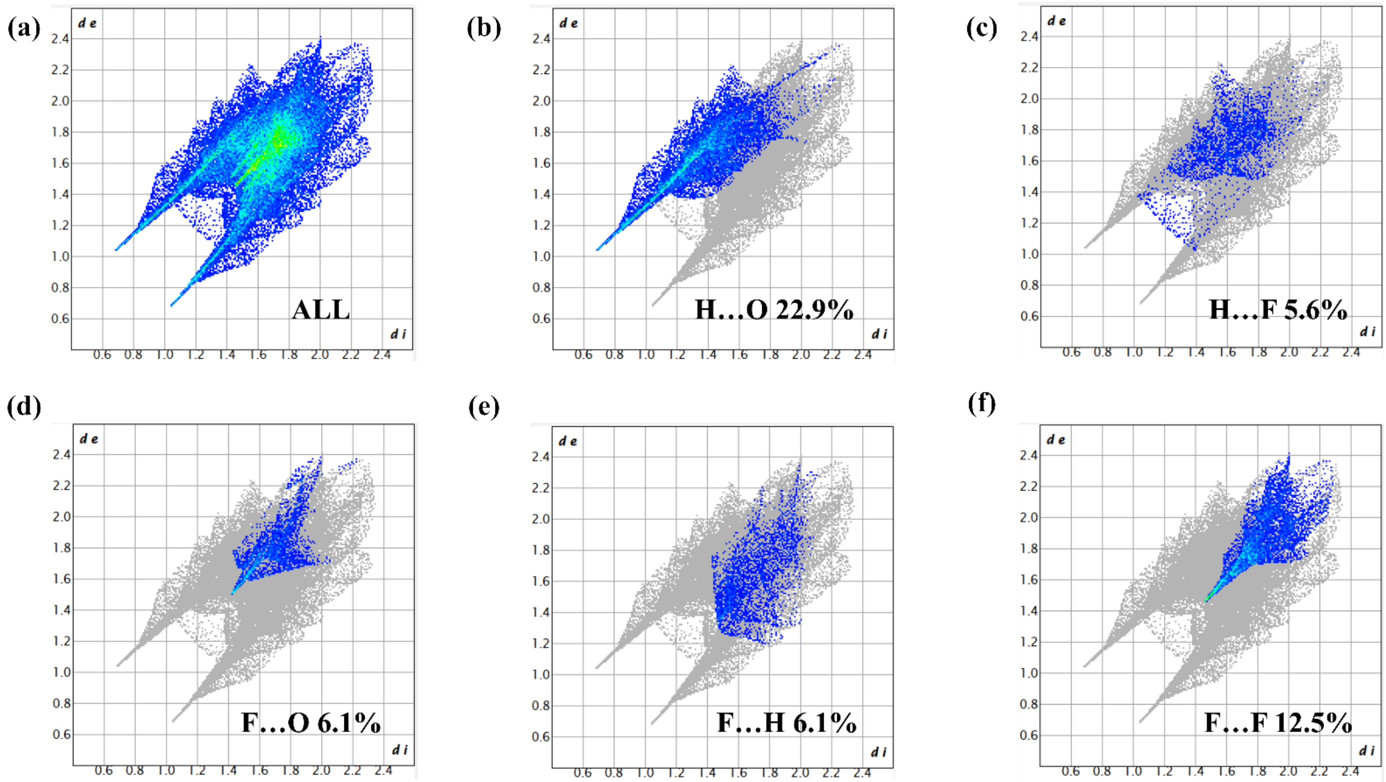

A). I

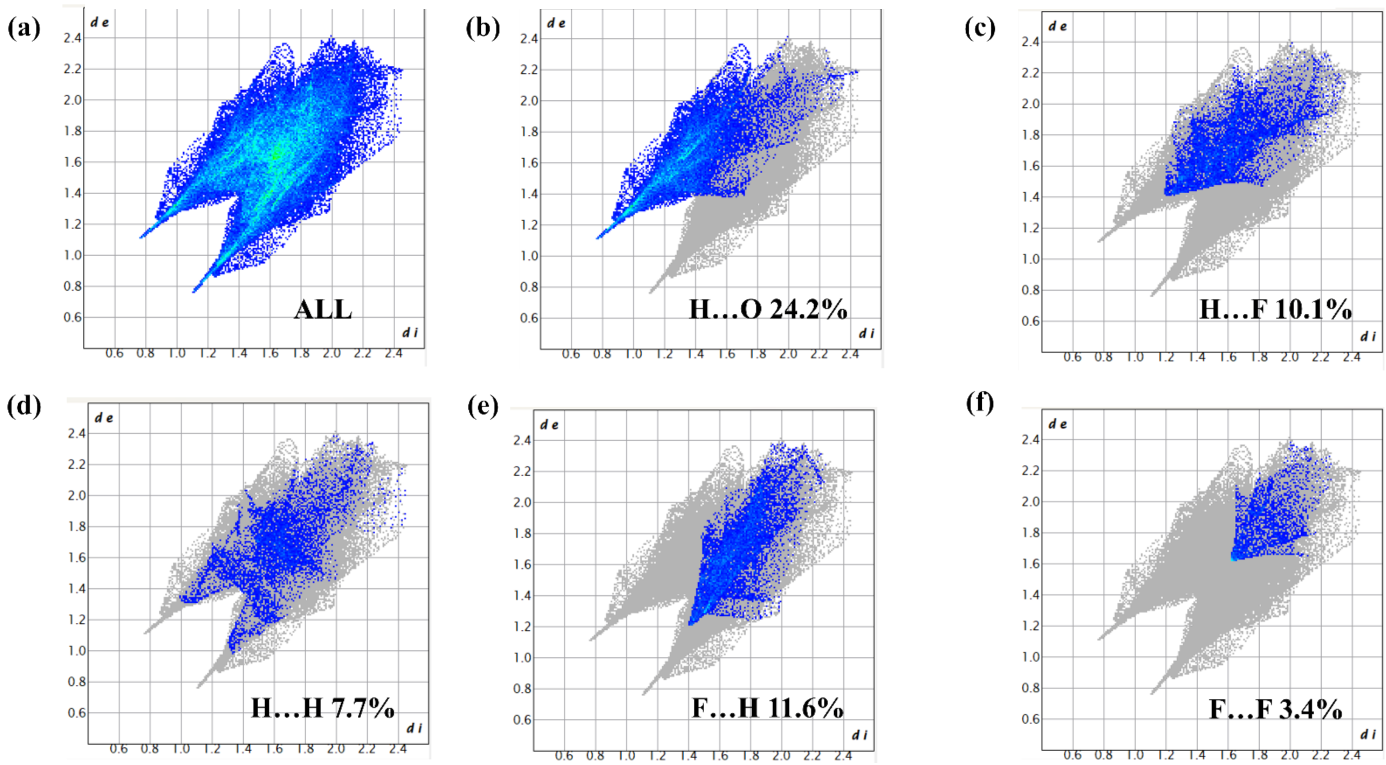

B). II

Fig. S9 Electronic structure calculated by GGA, total and partial density of states of a,c). **I**, b,d). Ⅱ.

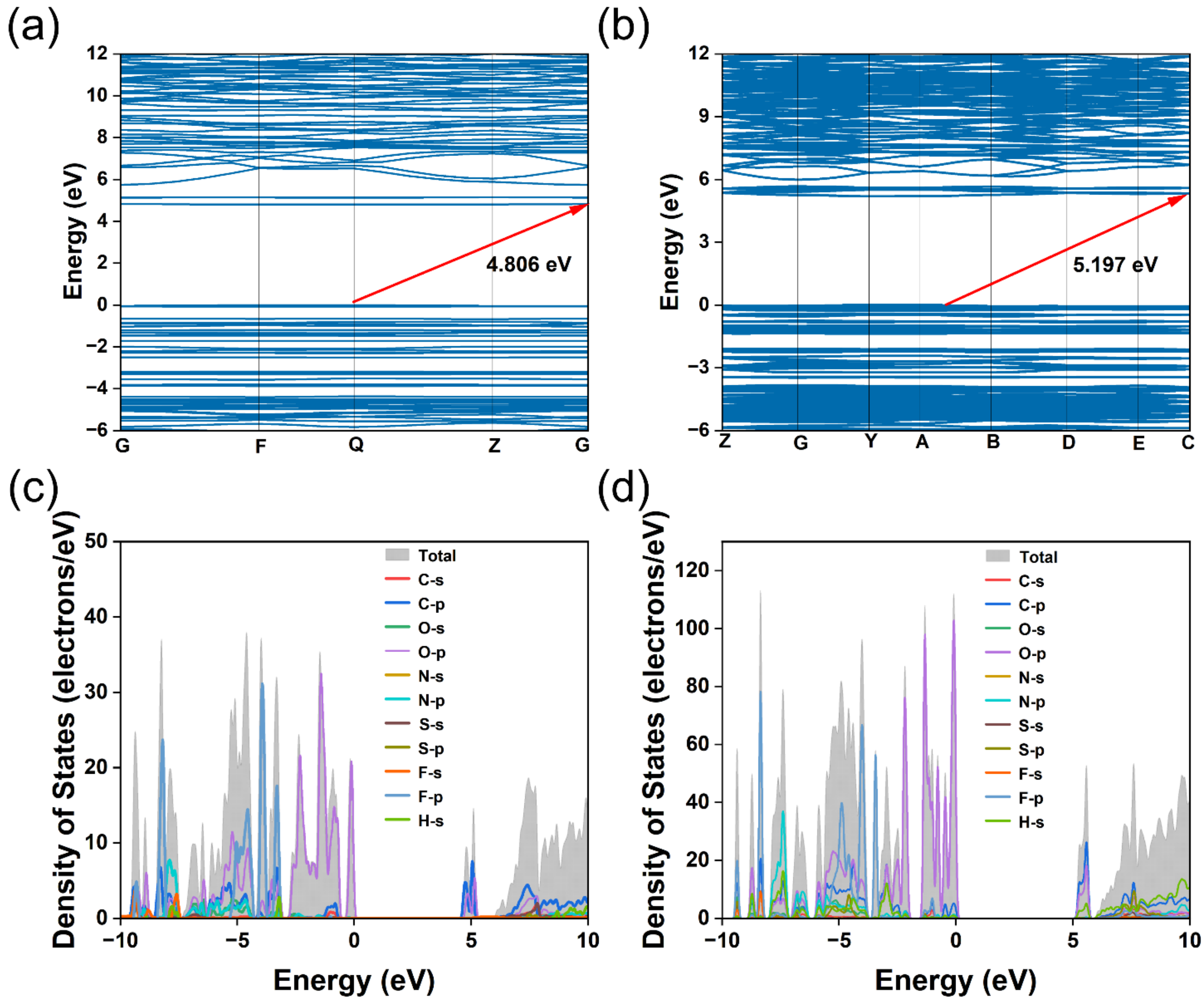

Fig. S10 The electron localization function diagrams for virtual electron's occupied and unoccupied states

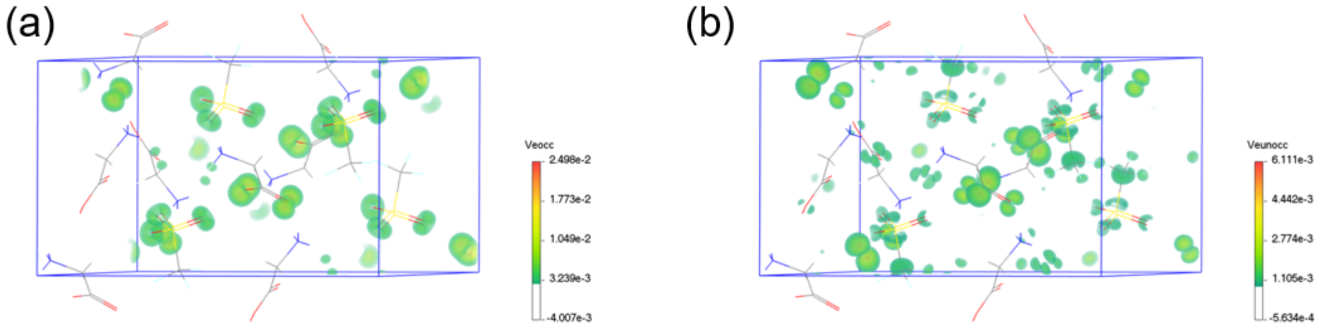

for d_{15} in Ⅱ.

References

1. [1] SAINT, Version 7.60A, Bruker Analytical X-Ray Instruments, Inc, Madison, WI 2008.
2. O. V. Dolomanov, L. J. Bourhis, R. J. Gildea, J. A. K. Howard, H. Puschmann, *OLEX2*: A Complete Structure Solution, Refinement and Analysis Program, *J. Appl. Crystallogr.*, 2009, **42**, 339-341.
3. a) P. R. Spackman, M. J. Turner, J. J. McKinnon, S. K. Wolff, D. J. Grimwood, D. Jayatilaka, M. A. Spackman, *CrystalExplorer*: A Program for Hirshfeld Surface Analysis, Visualization and Quantitative Analysis of Molecular Crystals, *J. Appl. Crystallogr.* 2021, **54**, 1006-1011; b) M. A. Spackman, D. Jayatilakaa, Hirshfeld Surface Analysis*, CrystEngComm*., 2009, **11**, 19-32.
4. S. J. Clark, M. D. Segall, C. J. Pickard, P. J. Hasnip, M. J. Probert, K. Refson, M. C. Payne, Z. Kristallogr, A First Principles Simulation Framework for the Interactions between a Si(001) Surface and a Scanning Probe, *Cryst. Mater*., 2005, **220**, 567-570.
5. W. Kohn, Nobel Lecture: Electronic Structure of Matter-Wave Functions and Density Functionals. *Mod. Phys*., 1999, **71**, 1253-1266.
6. J. P. Perdew, A. Zunger, Self-Interaction Correction to Density-Functional Approximations for Many-Electron Systems, *Phys. Rev. B*., 1981, **23**, 5048-5079.
7. A. M. Rappe, K. M. Rabe, E. Kaxiras, J. D. *Joannopoulos,* Optimized Pseudopotentials, *Phys. Rev. B*. 1990, **41**, 1227-1230.
8. Heyd, G. E. Scuseria, M. Ernzerhof, Hybrid Functionals Based on a Screened Coulomb Potential,*J. Chem. Phys.,* 2003, **118**, 8207-8215.
9. M. J. Frisch, G. Trucks, H. B. Schlegel, G. E. Scuseria, M. A. Robb, J. Cheeseman, G. Scalmani, V. Barone, B. Mennucci, G. A. Petersson, et al. Gaussian 09 Revision A.1. Gaussian Inc. 2009.
10. P. J. Stephens, F. J. Devlin, C. F. Chabalowski, M. J. Frisch, Theoretical Calculation of Vibrational Circular Dichroism Spectra, *J. Phys. Chem.,* 1994, 98, 11623-11627.
11. W. J. Hehre, R. Ditchfield, and J. A. Pople, Self-Consistent Molecular Orbital Methods. XII. Further Extensions of Gaussian-Type Basis Sets for Use in Molecular Orbital Studies of Organic Molecules, *J. Chem. Phys.,*1972, **56**, 2257-2261.
12. B. Xu, P. Gong, F. Liu, X. Zhang, H. Huo, Z. Lin, $(SO_3CF_3)^-$: A Non-π-Conjugated Motif for Nonlinear Optical Crystals Transparent into the Deep-Ultraviolet Region, *Adv. Opt. Mater*., 2024, **12**, 2301725.
13. X. Hao, M. Luo, C. Lin, G. Peng, F. Xu, N. Ye, $M(NH_2SO_3)_2$ (M=Sr, Ba): Two Deep-Ultraviolet Transparent Sulfamates Exhibiting Strong Second Harmonic Generation Responses and Moderate Birefringence.*Angew. Chem. Int. Ed*., 2021, **60**, 7621.
14. D. Dou, B. Cai, B. Zhang, Y. Wang, $M(NH_2SO_3)_2{\cdot}xH_2O$ (M = Ca, Pb, x = 0, 1, 4): Effect of Hydrogen Bonding on Structural Transformations and Second Harmonic Generation of Metal Sulfamates, *Inorg. Chem.,* 2022, **61**, 21131.
15. X. Wang, J. Lee, Y. Li, Y. Kuk, K. M. Ok, $Cd(NH_2SO_3)_2{\cdot}xH_2O$ (x = 0, 2): New Sulfamates with a Unique Coordination Environment and Reversible Phase Transitions, *Inorg. Chem. Front.,* 2023, **10**, 1411.

16. H. Tian, C. Lin, X. Zhao, F. Xu, C. Wang, N. Ye, M. Luo, $Ba(SO_3CH_3)_2$: A Deep-Ultraviolet Transparent Crystal with Excellent Optical Nonlinearity Based on a New Polar Non-π-Conjugated NLO Building Unit $SO_3CH_3^-$, *CCS Chem.*, 2023, **5**, 2497.
17. X. Wang, X. Leng, Y. Kuk, J. Lee, Q. Jing, K. M. Ok, Deep-Ultraviolet Transparent Mixed Metal Sulfamates with Enhanced Nonlinear Optical Properties and Birefringence, *Angew. Chem. Int. Ed.*, 2024, **63**, e202315434.
18. X. Wang, Y. Li, Z. Chen, J. Lee, F. Zhang, S. Pan, K. R. Poeppelmeier, K. M.Ok, $Sr(NO_3)(NH_2SO_3)\cdot H_2O$: First Nitrate Sulfamate Revealing Remarkable Second Harmonic Generation and Optimized Birefringence, *Small Struct.*, 2023, **4**, 2300274.
19. Y. Song, C. Lin, X. Zhao, T. Yan, N. Ye, H. Tian, M. Luo, Synergistic Combination of Different Types of Functional Motif in $Rb(NO_3)(SO_3NH_3)$ for Realizing Excellent Ultraviolet Optical Nonlinearity, *Inorg. Chem. Front.*, 2024, **11**, 4329.
20. M. Luo, C. Lin, D. Lin, N. Ye, Rational Design of the Metal-Free $KBe_2BO_3F_2$·(KBBF) Family Member $C(NH_2)_3SO_3F$ with Ultraviolet Optical Nonlinearity, *Angew. Chem. Int. Ed.*, 2020, **59**, 15978.
21. C. Hu, H. Li, G. Xu, Z. Yang, J. Han, S. Pan, The New Paradigm of Ligand Substitution-Driven Enhancement of Anisotropy from SO_4 Units in Short-Wavelength Region, *ACS Cent. Sci*. 2024, **10**, 2312.
22. Z. Bai, K. M. Ok, Designing Sulfate Crystals with Strong Optical Anisotropy through π-Conjugated Tailoring, *Angew. Chem. Int. Ed.*, 2024, **63**, e202315311.
23. X. Wen, Y. Yan, J. Lu, X. Shi, P. Tang, J. Chen, G. Yang, G. Peng, H. Yu, H. Zhang, Z. Hu, J. Wang, N. Ye, $[C_2N_4H_7O][NH_2SO_3]$: High-Performance Ultraviolet Nonlinear Optical Crystal with Ditrigon Coupled Guanylurea Group, *Angew. Chem. Int. Ed.*, 2025, **64**, e202424153.
24. Z. Zhang, X. Liu, R. Wang, S. Zhao, W. He, H. Chen, X. Deng, L. Wu, Z. Zhou, L. Chen, Remarkable Second Harmonic Generation Response in $(C_5H_6NO)^+(CH_3SO_3)^-$: Unraveling the Role of Hydrogen Bond in Thermal Driven Nonlinear Optical Switch**,** *Angew. Chem. Int. Ed.*, 2024, **63**, e202408551.